Applied Catalysis B: Environmental 163 (2015) 393–403

Contents lists available at ScienceDirect

Applied Catalysis B: Environmental

journal homepage: www.elsevier.com/locate/apcatb

Kinetic modeling of NH_3-SCR over a supported Cu zeolite catalyst using axial species distribution measurements

Xavier Auvray[a], William Partridge[b], Jae-Soon Choi[b], Josh Pihl[b], Filipa Coehlo[a], Aleksey Yezerets[c], Krishna Kamasamudram[c], Neal Currier[c], Louise Olsson[a,*]

[a] Chemical Engineering, Competence Centre for Catalysis, Chalmers University of Technology, Gothenburg, Sweden
[b] Fuels, Engines, and Emissions Research Center, Oak Ridge National Laboratory, P.O. Box 2008, MS-6472, Oak Ridge, TN 37831-6472, USA
[c] Cummins Inc., 1900 McKinley Ave, MC 50183, Columbus, IN 47201, USA

ARTICLE INFO

Article history:
Received 23 April 2014
Received in revised form 25 July 2014
Accepted 2 August 2014
Available online 12 August 2014

Keywords:
NH_3 SCR
Kinetic modeling
Spatial distribution measurements
Cu zeolites
Spaci-MS

ABSTRACT

In this study, a kinetic model is developed for NH_3-SCR over a honeycomb-monolith-supported Cu-zeolites using intra-catalyst axial species distribution measurements. An ammonia TPD experiment, together with micro calorimetry data were used for tuning the ammonia adsorption and desorption properties. The spatial distribution for NO oxidation, NH_3 oxidation and NH_3 "Standard" SCR were modeled between 200 and 400 °C. Four-step protocol measurements were employed in order to validate the transient functions of the model. The resulting kinetic model provides good spatiotemporal simulation of the SCR reaction and component reactions throughout the monolith catalyst system.

1. Introduction

With the depletion of fossil fuel resources and global warming, diesel and lean-burn gasoline engines are increasingly preferred for their advantageous fuel consumption and CO_2 emissions. On the other hand, they suffer from high NO_x emissions that contribute to global acidification and air pollution in urban environments. There are different concepts investigated for the catalytic reduction of NO_x into H_2O and N_2. In one technology, urea is injected into the exhausts gas to form NH_3, which is used as a reductant. The selective catalytic reduction (SCR) of NO_x proceeds on a downstream catalyst. In the quest for an efficient, cheap and non-toxic catalyst for this application, special attention has been given to metal-exchanged zeolites[1–6]. Zeolite catalysts are complex since they contain many sites with different properties and activity. The incorporation of metal atoms into the zeolite framework increases this degree of complexity due to the various potential oxidation states of the metal and the heterogeneity of the reactive sites. NH_3-SCR of NO_x itself is a complex catalytic reaction which can be described by many pathways depending on the NO_2/NO ratio [3,7] and is often accompanied by side reactions such as NH_3 oxidation, ammonium nitrate formation [8–10] and N_2O production [11]. Spatially resolved experiments have been performed to understand NH_3-SCR over monolithic catalysts with SpaciMS [12] and Spaci-FTIR [13,14]. Luo et al. [14] investigated SCR over a Fe/zeolite catalyst and observed that the catalyst zone required to meet 80% conversion decreases according to Standard SCR > NO_2-SCR > Fast SCR; i.e., Fast SCR requires the shortest catalyst length. With increasing temperature up to 400 °C, which is in line with observations over a Cu/zeolite catalyst [12], the SCR catalytic zone shifts to the front. In addition, Auvray et al. [12] provided information on the NH_3 adsorption and storage throughout the catalyst in SCR condition and observed NH_3 inhibition at low temperature in the front of the monolithic catalyst.

Global and detailed kinetic models have been built and developed to understand the NH_3-SCR reaction over the most common catalysts: supported-vanadia catalysts [10,15], Fe-exchanged zeolites [16] and Cu-exchanged zeolites [17]. These models include side reactions, several possible routes for NO_x reduction, such as "Standard SCR", "Fast SCR" and "NO_2 SCR"[17], or those focused on the nature and dynamics of the active sites [18–21]. Catalysts for NO_x-selective reduction are practically coated onto a monolithic support and this system behaves like a plug flow reactor along which chemical species concentrations evolve according to

* Corresponding author. Tel.: +46 31 772 4390; fax: +46 31 772 3035.
E-mail address: louise.olsson@chalmers.se (L. Olsson).

http://dx.doi.org/10.1016/j.apcatb.2014.08.003
0926-3373/

reactions, adsorption and release. The models found in the literature are built, fitted and validated based on effluent concentrations under various operating conditions. There is one kinetic model available in the literature that is describing spatially resolved MS data for NO_x storage and reduction [22]. However, there are to our knowledge, no kinetic models available for NH_3 SCR that uses spatially resolved experiments. In-catalyst distributed measurements enable kinetic parameters to be determined under actual operating conditions, during which regular data for NH_3 SCR yield substantial conversion (often 100%) in a significant part of the temperature interval. Thus, there are large advantages of using spatially resolved measurements. The objective of this study has been to develop a kinetic model for NH_3-SCR using intra-catalyst concentration profiles of species relevant to the process. NH_3 oxidation, NO oxidation, Standard NH_3-SCR, N_2O formation, as well as NH_3 adsorption and desorption, have been included in the model. The validation of the model was performed by evaluating its capability to capture transient response to changes in the gas composition, i.e. switching NH_3 or NO on or off.

2. Experimental

2.1. Catalyst

The catalyst used was a Cu-Beta, also denoted Cu-BEA, zeolite prepared as described in [23,24] and washcoated on a 400-cpsi monolithic cordierite support. The silica-to-alumina ratio was 38 and was prepared using Beta zeolite from Zeolyst International. The copper content was 4.3 wt.%, as measured by inductively coupled plasma and atomic emission spectrometry (ICP-AES). A cylindrical catalyst core sample (25.4-mm long × 7.1-mm diameter) was used for micro reactor analysis. The catalyst was pretreated for 2 h at 500 °C in a gas stream containing 205 ppm NO, 183 ppm NH_3, 10% O_2, 5% H_2O and Ar balance, to simulate SCR exhaust conditions; this treatment ensures sample thermal stability during subsequent experiments.

2.2. Reactor setup and analytical technique

The system used to perform the experimental work has been described in detail in a previous article [12]. The catalyst core sample was wrapped in fiber glass insulation tape in order to minimize gas flow bypassing the catalyst and was placed in a quartz tube positioned in a reactor furnace. Quartz rods were placed in the tube upstream and downstream from the catalyst to reduce axial temperature gradients within the sample (only ±1 °C over the 25.4-mm long catalyst). Gases were supplied by mass flow controllers and were preheated and mixed before entering the flow reactor in coiled tubing enclosed in a separate preheater furnace. All the gas lines were maintained at >200 °C and the catalyst internal temperature was measured by a K-type thermocouple inserted in the sample ca. mid-monolith from the reactor outlet. Analysis of the intra-catalyst gas composition was performed using SpaciMS, an instrument described elsewhere [25–29]. One fused-silica capillary (Polymicro Technologies, 50-μm I.D., 185-μm O.D., ca. 2-m long) was inserted in the monolith from the inlet and mounted on a translating system to sample the gas at any position along the channel. A second capillary was inserted in the reactor to measure the inlet gas composition. The capillaries were connected to a multiport valve, the outlet of which was linked to the mass spectrometer inlet. Thus, switching the valve allowed selecting the gas feed for the mass spectrometer. The capillaries were maintained at ca. >200 °C throughout their entire length. The experiment was carried out at the catalyst exit and six target intra-catalyst locations: 1/2, 3/8, 1/4, 3/16, 1/8 and 1/16 of the total monolith length. For the exit measurement, the capillary was actually positioned just inside the catalyst outlet; this allowed exclusive sampling from the measurement catalyst channel and not adjacent channels, which would complicate the analysis due to channel-to-channel performance (e.g., washcoat loading) differences. The experimental sampling positions were corrected using ammonia oxidation and SCR conversion as described in detail in [12]. The *m/z* ratios monitored were 15 for NH_3, 28 for N_2, 30 for NO, 44 for N_2O, 46 for NO_2 and 84 for Kr; despite these signal assignments, there were numerous cross sensitivities which were considered in our analysis.

2.3. Experimental procedure

The Cummins 4-step protocol [30] was used for analysis and consists of four successive steps at constant flow and temperature:

- Step 1 (NO oxidation): 205 ppm NO, 10% O_2 and 5% H_2O in Ar.
- Step 2 (Standard SCR): 205 ppm NO, 183 ppm NH_3, 10% O_2 and 5% H_2O in Ar.
- Step 3 (NH_3 Saturation): 183 ppm NH_3, 10% O_2 and 5% H_2O in Ar.
- Step 4 (NO oxidation): 205 ppm NO, 10% O_2 and 5% H_2O in Ar.

A low concentration of Kr was included for analytical purposes. The total flow was 510 sccm (0 °C and 760 Torr standard conditions) providing a space velocity of 30,000 h^{-1}. To assess repeatability, the 4-step protocol was repeated twice at each location and temperature, and the second step was typically used for analysis. The catalyst nature was studied at 200, 325 and 400 °C. Fig. 1 shows typical experimental concentration profiles obtained during the protocol described above. The nitrogen balance was also added in order to verify the stoichiometry of the various reactions. It can be seen that the N-balance was closed during all steps.

3. Model

3.1. Reactor model

The model aims at reproducing the intra-catalyst evolution of the reactions occurring during NH_3-SCR. To simulate the behavior of a honeycomb-type catalytic converter, the "aftertreatment analysis" mode of a commercial software, AVL BOOST, was used. The dimensions of the monolith used led to the following geometric surface area, GSA = 2649.6 $m^2/m_{monolith}$. In order to optimize the computation time, several assumptions were made. All the channels were assumed similar, which reduced the system to a one dimension single channel model. The 1D channel was discretized into 15 elements in a series, in which the mass balance (Eq. (1)) equation was solved [31].

$$\varepsilon_g \times \frac{\partial \rho_g \times w_{k,g}}{\partial t} = \varepsilon_g \times \frac{\partial \rho_g \times w_{k,g} \times v_g}{\partial z} + \varepsilon_g \times \frac{\partial}{\partial z}\left(\rho_g \times D_{eff} \times \frac{\partial w_{k,g}}{\partial z}\right) + MG_{k,g} \times \sum_{i}^{I} \nu_{i,k} \times \dot{r}_i(c_k^L, T_s) \quad (1)$$

ε_g is the volume fraction of the gas phase in entire system, ρ_g the density of the gas phase (kmol/m^3), $w_{k,g}$ the mass fraction of species k in gas phase, $\nu_{i,k}$ the stoichiometric coefficient of species k in reaction i, $\dot{r}_i(c_k^L, T_s)$ represents the molar reaction rate of the surface reaction i, and $MG_{k,g}$ is the molar mass of gas phase species k (kg/kmol). The transport of species from the bulk gas phase to the surface was included and described by the film model. Thus,

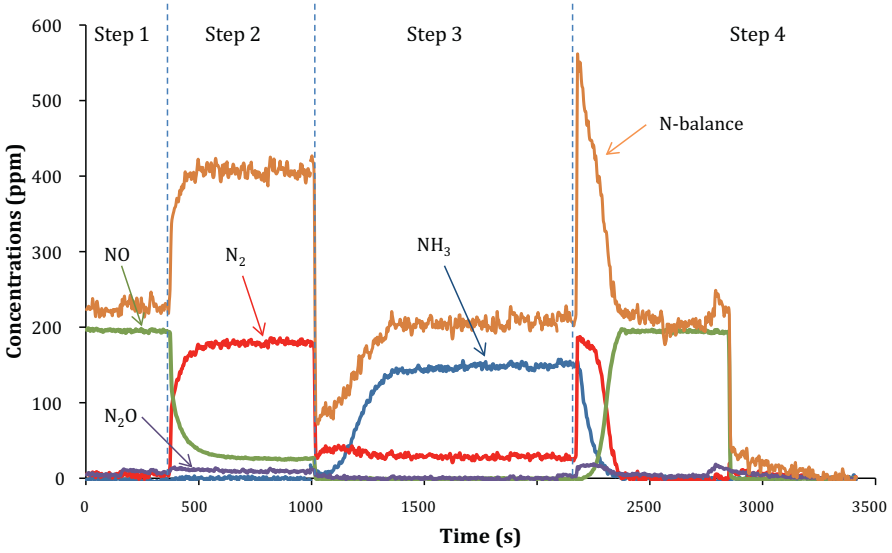

Fig. 1. Concentrations of NO, NH_3, N_2 and N_2O measured during the 4-step protocol at 325 °C and at the half of a Cu-BEA monolith. The nitrogen balance was calculated and also represented on the figure.

the molar surface concentration (c_k^L of the component k) can be evaluated using

$$a_{trans} \times k_{k,m} \times (c_k^L - c_{k,g}) = \sum_i^I \dot{r}_i \times (c_k^L, T_s) \quad (2)$$

where $c_{k,g}$ is the molar concentration of species k in the bulk gas, and $k_{k,m}$ is the mass transfer coefficient of the individual species. Considering the low working temperature range, homogeneous gas phase reactions were neglected in the model.

The reaction heat associated with NH_3 SCR is small and, therefore, the simulations were considered isothermal, which also was the case in several earlier NH_3 SCR models [16–22].

BOOST allows the user to define the axial position of the simulation output. This option was convenient and enabled us to extract the simulated concentrations at the axial positions where the capillary inlet was experimentally placed for easy comparison purposes.

3.2. Kinetic model

The rate equations and kinetic parameters were user-defined in a FORTRAN script executed by BOOST. The rate constants were described by the Arrhenius Equation:

$$k = A \exp\left(-\frac{E_A}{RT}\right) \quad (3)$$

Table 1
Equations and kinetics parameters for NH_3 adsorption and desorption from TPD experiments.

Reaction	Equation/reaction rate	Pre-exponential factor[a] (kmol/(m³ s))	Activation energy (kJ/mol)	Variance (s^2)
NH_3 adsorption	$NH_3 + S1 \rightarrow NH_3\text{-}S1$ (r.1f) $r_{1f} = k_{1f} \times \theta_v \times [NH_3]$	9279[b]	0	1091
NH_3 desorption	$NH_3\text{-}S1 \rightarrow NH_3 + S1$ —(r.1b) $r_{1b} = k_{1b} \times \theta_{S1-NH_3}$	6.8×10^8[b]	113.0[c]	

[a] The unit for the reaction rate is kmol/(m³ s) and the gas phase concentrations are dimensionless.
[b] Fitted.
[c] Parameters from micro-calorimetry experiments. $\alpha = 0.39$.

Table 2
Estimated kinetic parameters for NO oxidation, step 1 of the 4-step protocol.

Reaction	Equation/reaction rate	Pre-exponential factor [a] (kmol/(m³ s))	Activation energy (kJ/mol)
NO oxidation[c]	$NO + 0.5O_2 \Leftrightarrow NO_2$ (r.2) $r_2 = k_{2f} \times [NO] \times [O_2]^{0.5} - k_{2b} \times [NO_2]$	2.5×10^4[b]	39.6 [34]

[a] The unit for the reaction rate is kmol/(m³ s) and the gas phase concentrations are dimensionless.
[b] Fitted.
[c] Parameters for forward reaction, backward reaction from thermodynamic equilibrium.

Table 3
Estimated kinetic parameters for NH_3 oxidation, step 3 of the 4-step- protocol.

Reaction	Equation/reaction rate	Pre-exponential factor[a] (kmol/(m³ s))	Activation energy (kJ/mol)
NH_3 oxidation	$4NH_3\text{-}S1 + 3O_2 \rightarrow 2N_2 + 6H_2O + 4S1$ (r.3) $r_3 = k_3 \times \theta_{S1-NH_3} \times [O_2]^{\beta_1}$	3.0×10^6[b]	99.5 [34]

[a] The unit for the reaction rate is kmol/(m³ s) and the gas phase concentrations are dimensionless.
[b] Fitted.

Table 4
The variance calculated for steady-state NH_3 oxidation and SCR. All components involved in the respective reactions were taken into account in the calculations.

Reaction temperature	NH_3 oxidation	SCR
200 °C	–	270
325 °C	1489	1040
400 °C	229	398

where A is the pre-exponential factor, E_A the activation energy (J/mol), R the gas constant (8.314 J/(mol K)) and T is the temperature (K). The pre-exponential factor and the activation energy of each simulated reaction were tuned to fit the experimental data and are tabulated (Tables 1–5).

3.2.1. NH_3 adsorption and desorption

The model included NH_3 adsorption and desorption on catalytic sites of the Cu-BEA, denoted S1 (see Table 1). It was considered to be a non-activated step and the activation energy of adsorption was set at 0, which has been the case in many NH_3 SCR models [16,17]. Unlike adsorption, the ammonia desorption is an activated process, the activation energy of which is coverage dependent. The activation energy of NH_3 desorption was expressed using a Temkin isotherm, which considers the adsorbate–adsorbate interactions:

$$E_{NH_3,des} = E^0_{NH_3,des}(1 - \alpha\theta_{NH_3}) \quad (4)$$

where α is a constant fitting parameter, θ_{NH_3} the NH_3 coverage and $E^0_{NH_3,des}$ is the activation energy for 0 coverage. An alternative explanation for the coverage dependent activation energy is that in zeolites there is a range of acidity for the sites, and a coverage dependent barrier reflects this inhomogeneity. A coverage dependent activation energy for NH_3 desorption has been used in many kinetic models [16,19,20,32] and is in line with micro-calorimetric experiments by Wilken et al. [23]. Micro-calorimetry experiments on Cu-BEA powder from the same batch as is used in this study resulted in an adsorption heat of 112.75 kJ/mol with a coverage-dependence α of 0.39. These values were used in the model. NH_3 adsorption followed by TPD was performed in order to experimentally measure the number of sites and to fit the adsorption/desorption parameters, which are reported in Table 1. Since no storage of nitric oxide was observed, even at 200 °C, NO adsorption was not taken into account.

3.3. NH_3 and NO oxidation

Zeolites are active for oxidation of NO and NH_3 [6,33]. Oxidation of NH_3 by oxygen leads to an overconsumption of NH_3 [14] while NO_2, produced by NO oxidation, improves the SCR process via the "Fast SCR" mechanism. The oxidation of NH_3 was modeled according to the reaction of NH_3, adsorbed on S1, and O_2 present in the gas phase. However, this is a global model, which does not imply that the oxygen is physically reacting from the gas phase. The only product formed during the experiment was N_2, and therefore only one reaction was included in the model to describe ammonia oxidation. The steady-state concentrations of NH_3 and N_2 at various intra-catalyst axial positions during Step 3 were used to tune the parameters. The tuning of NO oxidation parameters followed the same approach. In the model, NO oxidation was described as a global reaction dependent on NO and O_2 concentration (Table 2). In the same way as for NH_3 oxidation, this is a global kinetic model using gas phase concentrations but in reality, the reaction occurs on the surface. These two reactions were studied independently to determine their kinetic parameters, which were subsequently used in the simulation of NH_3 SCR and among the entire range of 4-step experiments aiming at validating the model. The activation energies were taken from the experimental kinetic study by Mihai et al. [34] over a Cu-BEA catalyst containing 4 wt.% Cu. The pre-exponential factors were determined by manual tuning.

3.4. NH_3 SCR

NH_3 SCR in excess oxygen was modeled according to only one reaction corresponding to the "Standard SCR". The "Fast SCR" and the NO_2-SCR reactions were excluded to simplify the model since NO_2 was not present in the gas feed and NO oxidation was significant only at 400 °C, albeit at a significantly lower rate compared to NH_3 SCR. The activation energy for NH_3 SCR was taken from Arrhenius experiments presented by Mihai et al. [34] and the pre-exponential factor was manually tuned, similar to the NO and NH_3 oxidation reactions, to fit the experimental steady state distributed concentrations of N_2, NH_3, and NO. Since NO oxidation and NH_3 oxidation may occur during lean SCR conditions, these reactions were accounted for in the modeling of the SCR step using the parameters determined in these previous sub-models.

3.5. N_2O formation

During SCR of NO with NH_3, the formation of N_2O has been observed on various metal-exchanged zeolite catalysts [3,8,11]. Several pathways have been proposed for the N_2O formation. There is a correlation between NO_2 and N_2O since the production of the latter increases with NO_2 concentration [3,4]. N_2O release has been explained by the formation and subsequent decomposition of ammonium nitrate, the direct oxidation of NH_3 or SCR with a different stoichiometry. These side reactions should be avoided since they consume NH_3 and produce N_2O, the emission of which is an environmental issue due to its significant greenhouse gas potential. The type of SCR catalyst and its operating temperature are among the factors influencing N_2O selectivity. On Cu-BEA zeolites, a high N_2O selectivity at low temperature (200 °C) as well as high (400 °C) temperature has been noticed [12]; however, at 325 °C, the N_2O formation was lower. Two pathways were therefore included in our model to simulate the N_2O production: the low-temperature pathway, involving the formation of an adsorbed NH_3-NO complex, and the high-temperature pathway, involving a reaction between adsorbed NH_3 and NO (see Table 5). The reaction mechanism for N_2O production used in this paper was developed in an earlier study, using a broad range of temperatures and a varying NO_2/NO_x ratio [35].

Table 5
Equation and estimated kinetic parameters for ammonia SCR, step 2 of the 4-step protocol.

NH_3 SCR equation/reaction rate	Pre-exponential factor[a] (kmol/(m³ s))	Activation energy (kJ/mol)
$4NH_3$-S1 + $4NO + O_2 \rightarrow 4N_2 + 6H_2O$ + 4S1 (r.4) $r_4 = k_4 \times \theta_{S1-NH_3} \times [NO] \times [O_2]^{\beta_2}$	4×10^{13}[b]	107.8 [34]

[a] The unit for the reaction rate is kmol/(m³ s) and the gas phase concentrations are dimensionless.
[b] Fitted.

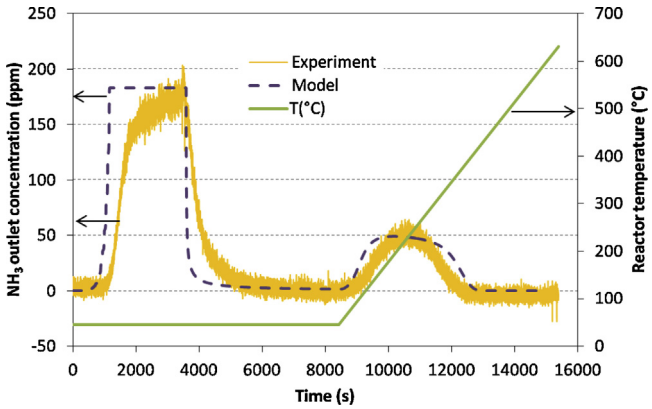

Fig. 2. NH_3 adsorption and temperature programmed desorption. The inlet ammonia concentration was 183 ppm and the temperature 40 °C (T_{cat} = 56 °C).

3.6. Model validation

Whereas the steady state distributed experimental data from the 4-step protocol were used to determine the kinetic parameters of the individual reactions, the transients associated with the various gas-composition steps in the protocol were used to validate the model. The entire protocol was therefore simulated and compared to the experimental results.

The variance was determined according to:

$$S^2 = \frac{\sum_i (C^k_{model,i} - C^k_{exp,i})^2}{N - p}$$

where N is the number of points considered, p the number of fitted parameters, $C^k_{model,i}$ the concentration of the species i calculated by the model at the position k and $C^k_{exp,i}$ is the measured concentration of the species i at the position k.

4. Results and discussion

4.1. NH_3 temperature programmed desorption (TPD)

The catalyst was exposed to a gas stream containing 183 ppm NH_3 at low temperature (40 °C) in order to store NH_3 until catalyst saturation. A fraction of the stored amount was released when NH_3 was removed from the flow, forming a long tail on the NH_3 profile, which is in line with earlier studies [17,32,36]. The temperature was progressively increased at 5 °C/min to 600 °C in order to release the remaining NH_3 stored during the exposure. The quantitative NH_3 outlet concentration profile is shown in Fig. 2. The amount of adsorbed and released ammonia was calculated and used to fit the number of active sites, which is a crucial parameter for the kinetic model. Adsorption was considered to be a non-activated step and the activation barrier was set to zero, as done in several other studies [19]. The pre-exponential factors for adsorption and desorption were fitted to reproduce the shape of the associated data in Fig. 2. Due to the interaction between ammonia molecules, or alternatively non-homogeneous strength of the acid sites, a coverage-dependent expression was used for the activation energy of desorption (Eq. (4)). As described in Section 3.2.1, the coverage dependent activation energy was determined using micro-calorimetry. The fitted parameters are reported in Table 1 and the results in Fig. 2 compare the experimental and simulated NH_3 TPD profiles. The model has a lower ammonia storage compared to the experiment and also there is a larger tailing of the ammonia concentration after turning it off. The reason is that the NH_3 adsorption preceding the TPD experiments was made at 40 °C, and at this low adsorption temperature it is possible that physisorbed ammonia is available on the catalyst, which was added in a kinetic model by Sjövall et al. [19] for SCR over Cu/ZSM-5. Since the activity of the catalyst was modeled at 200 °C and higher, the physisorbed ammonia was not taken into consideration in this study. The variance calculated for NH_3 over the curve showed in Fig. 2 was appended in Table 1. The number of S1 sites in the model was 0.0257 mol/m^2, i.e. 68.1 mol/m $_{monolith}$ (geometric surface area, GSA = 2649.6 m^2/m $_{monolith}$).

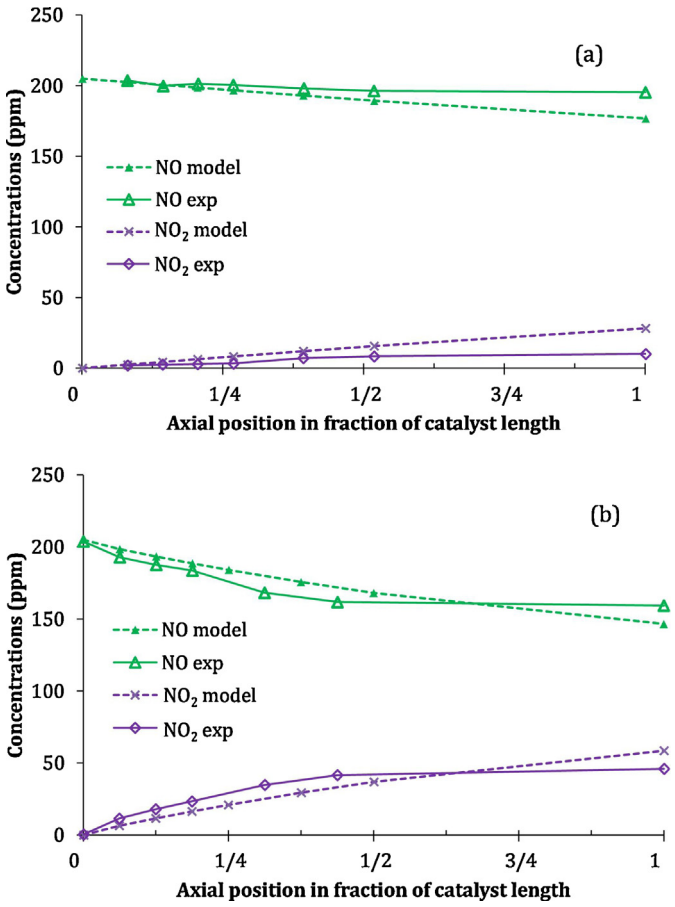

Fig. 3. NO oxidation (205 ppm NO, 10% O_2, 5% H_2O): experimental (solid lines) and simulated (dotted lines) intra-catalyst NO and NO_2 concentration profiles: (a) 325 °C and (b) 400 °C.

4.2. NO oxidation

In Step 1 of the 4-step protocol, NO was added together with oxygen and water vapor. Under these conditions, the oxidation of NO into NO_2 could take place provided that the temperature was high enough. The oxidation of some NO was observed at 400 °C (Fig. 3b) and, to a lesser extent, at 325 °C (Fig. 3a), whereas no activity was noted at 200 °C. The extent of the reaction could be measured along the catalyst and then modeled. The activation energy of 39.6 kJ/mol, reported by Mihai et al. [34] for NO oxidation over Cu-BEA catalyst containing 4 wt.% Cu, was used and yielded good agreement with the experimental data shown in Fig. 3. This value was close to the activation energy reported by Olsson et al. [17] on Cu-ZSM-5 (48 kJ/mol) and Metkar et al. on Fe-ZSM-5 (48 kJ/mol) and Cu-chabazite (56 kJ/mol) [32]. The model predicts a rather linear evolution of NO and NO_2 in the monolith, especially at 325 °C. However, the experiment conducted at 400 °C showed a linear evolution in the front half of the catalyst followed by a constant NO and NO_2 concentration in the rear half of the catalyst. The decrease in the NO oxidation rate experimentally observed

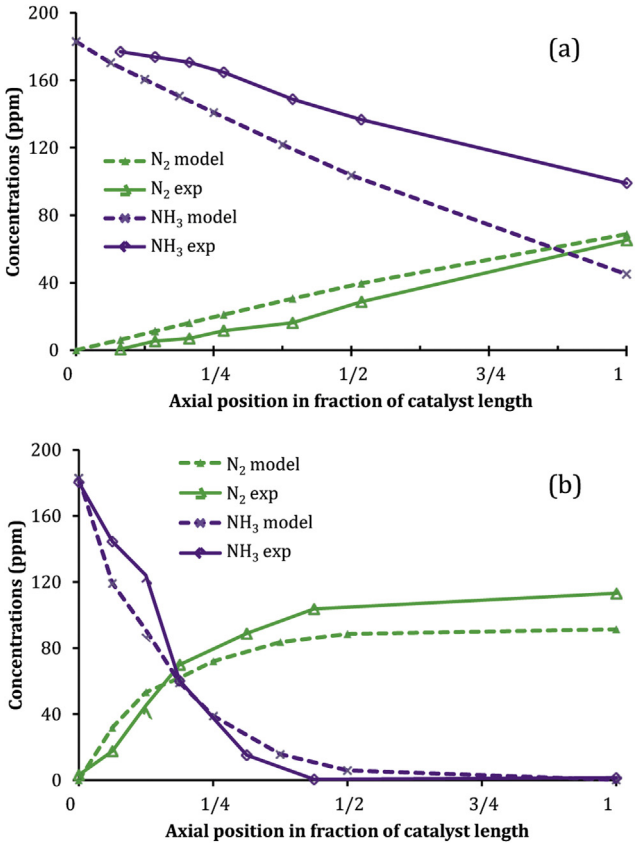

Fig. 4. NH_3 oxidation (183 ppm NH_3, 10% O_2, 5% H_2O): experimental (solid lines) and simulated (dotted lines) intra-catalyst NH_3 and N_2 concentration profiles: (a) 325 °C and (b) 400 °C.

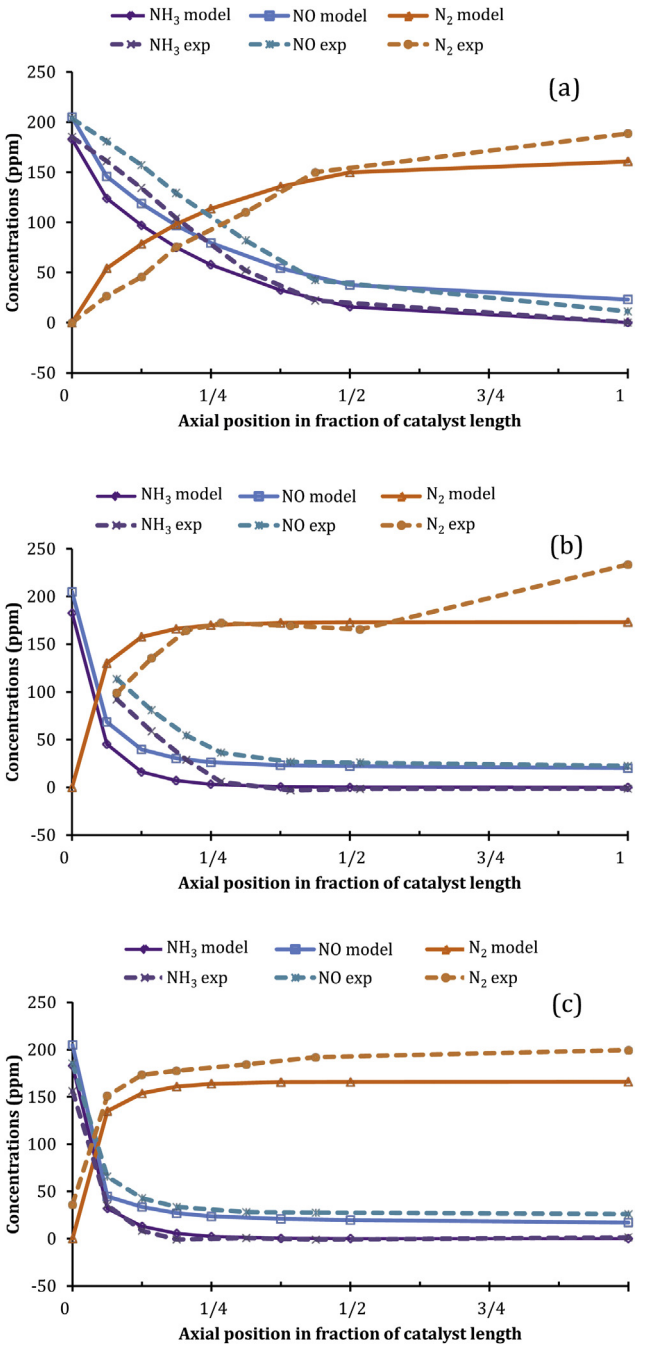

Fig. 5. NH_3-SCR (183 ppm NH_3, 205 ppm NO, 10% O_2, 5% H_2O): experimental (dotted lines) and simulated (solid lines) intra-catalyst NO, NH_3 and N_2 concentration profiles: (a) 200 °C, (b) 325 °C and (c) 400 °C.

at the monolith end is likely due to NO_2 inhibition of NO oxidation. This has been suggested for NO oxidation over Fe-ZSM-5 and Cu-chabazite [37]. Because the experiments were carried out feeding only NO, NO_2 inhibition was not included in the model; our intra-catalyst results suggest the necessity of including the inhibition effect and more data would be needed for describing the trend such as the apparently greater inhibition at 325 °C than at 400 °C. The parameters used in the simulation are shown in Table 2.

4.3. NH_3 oxidation

In the presence of O_2 and water, ammonia was oxidized on Cu-BEA at 325 and 400 °C. This reaction can occur in parallel during NH_3-SCR and it is therefore important to accurately determine its kinetic parameters. Fig. 4 shows the spatial evolution of NH_3 and nitrogen concentrations during Step 3 (NH_3 oxidation) at both 325 °C (Fig. 4 a) and 400 °C (Fig. 4b). The activation energy was fixed at a literature value [34]. Hence, by tuning only the pre-exponential factor, excellent agreement at both temperatures was difficult to obtain. Since the NH_3 oxidation was more significant at high temperature, the data obtained at 400 °C were the focus of the fitting procedure. At 325 °C, the parameters reported in Table 3 resulted in a slightly faster NH_3 consumption compared to the experimental results. It should be noted that, at 325 °C, the last experimental point (position = 1 catalyst length) shows an unexpectedly high N_2 value ($N_2/NH_{3,consumed} = 1.27$), which might be attributable to measurement uncertainties; nevertheless, all other NH_3 and N_2 data points from the experiments and modeling indicate the 2-to-1 NH_3:N_2 stoichiometry, which is given by reaction 3 in Table 3. At 325 °C, both the model and the experiments show a rather linear NH_3 consumption and N_2 formation along the monolith (Fig. 4a). At 400 °C, the concentrations evolved rapidly in the front half of the catalyst until full conversion was reached. The model was able to simulate intra-catalyst concentrations of N_2 and NH_3 during NH_3 oxidation adequately at 400 °C (Fig. 4b), with a variance below 230 (Table 4). At 325 °C, the model overestimated NH_3 oxidation and as a result, the variance calculated was high. Since the activation energy was fixed and NH_3 oxidation was modeled according to one single reaction following Arrhenius' kinetic law, the tuning of the reaction was limited to the pre-exponential factor. The activation energy value used for NH_3 oxidation (99.5 kJ/mol) was obtained by Mihai et al. using Arrhenius plots for 4% Cu/BEA. This value was

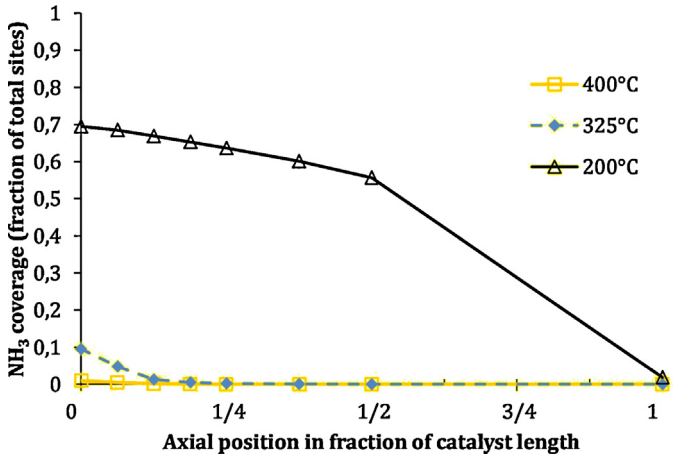

Fig. 6. Simulated NH_3 coverage and fraction of free sites during NH_3 SCR at: (a) 200 °C, (b) 325 °C and (c) 400 °C. Steady-state profile throughout the catalyst.

close to the 97.36 kJ/mol reported by Sjövall et al. [19] on Cu-ZSM-5. The reaction order of oxygen (β_1 in Table 3) was, in the simulations, 0.6 and was tuned to separate experiments with varying O_2 concentration (results not shown here).

4.4. NH_3 SCR

The parameters determined previously for NO and NH_3 oxidation as well as for NH_3 adsorption and desorption were held constant and used when tuning the NH_3-SCR parameters. The reaction order of oxygen (β_2 in Table 5) was determined as described for β1, and the value of 0.5 was used in the simulations. The catalyst was active for SCR at all three temperatures. In addition, side reactions occurred, yielding N_2O. However, due to the low NO oxidation activity, reactions involving NO_2, such as "Fast SCR" and NO_2 SCR", were not taken into account by the model. During the SCR step, ammonia is the key component since it is involved in NH_3 storage, NH_3 oxidation, NH_3-SCR and N_2O formation. A good agreement between the model and measurements was observed for the intra-catalyst concentration profiles of NH_3, NO and N_2. The experimental concentration profiles at 200 °C (Fig. 5a) show a rather linear evolution in the front half of the monolith. At 325 °C (Fig. 5b), this trend applies only through the front quarter of the catalyst where almost complete consumption of ammonia is reached. At both temperatures, the model slightly overestimates the reaction rate in the front of the catalyst. At 400 °C, the rapid consumption of NO and NH_3 in the catalyst front as well as the exponential shape of the profiles (Fig. 5c) are accurately reproduced by the model. The model slightly overestimates NO consumption throughout the catalyst whereas the gap between experimental and simulated N_2 profiles is mostly attributable to experimental uncertainties on N_2 measurements, leading to an N-balance of ≈110% throughout the entire catalyst. In general, the model agrees well with the SCR experimental data. The activation energy of SCR (107.8 kJ/mol) measured by Mihai et al. [34] was relatively high for a 4 wt.% Cu-BEA zeolite catalyst while lower values were obtained for Cu/BEA with lower copper loadings. The high activation energy resulted in a high pre-exponential factor in order for the SCR to occur at a significant rate at low temperature. Using this pre-exponential factor (4×10^{13} kmol/(m^3 s)) resulted in a good agreement of the model at 200 °C (Fig. 5a) and excellent results for the 400 °C case (Fig. 5c), data verified by the low variance at these temperatures (Table 4). Since the parameter optimization was based on the 200 and 400 °C, the agreement was less good at 325 °C in the front part of the catalyst (Fig. 5b).

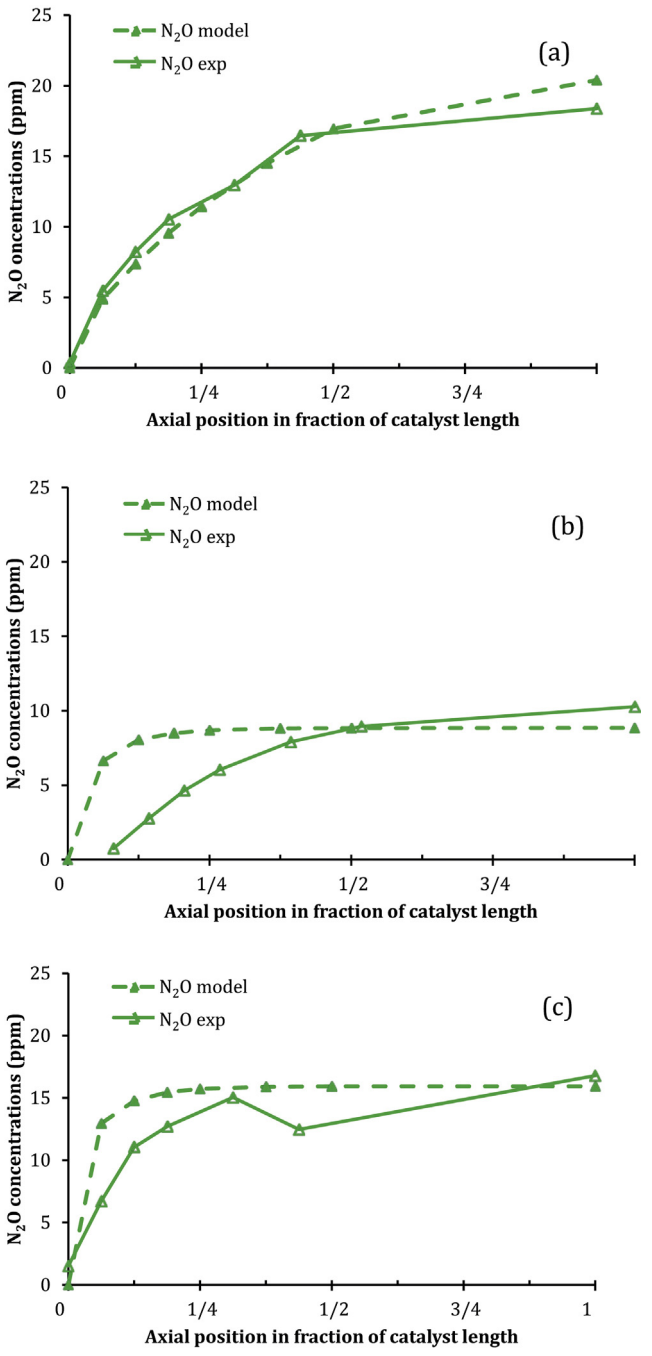

Fig. 7. N_2O formation as a by-product of NH_3-SCR. The inlet feed consisted in 183 ppm NH_3, 205 ppm NO, 10% O_2, 5% H_2O. Experiment (solid lines) and simulation (dotted lines) intra-catalyst N_2O concentration profiles: (a) 200 °C, (b) 325 °C and (c) 400 °C.

4.5. NH_3 coverage

The SCR catalyst is capable of storing ammonia as observed in our experiment during Steps 2 and 3. Simultaneously, our model includes the consumption of surface NH_3 by the reaction with NO and oxygen and the equilibrium of surface NH_3 with gas phase NH_3. According to these factors, NH_3 surface coverage, defined by the number of sites occupied by NH_3 divided by the total number of sites was calculated along the catalyst length. Fig. 6 presents the calculated NH_3 coverage during SCR (Step 2) at steady state. It was observed that ammonia coverage decreases through the catalyst

Table 6
Equations and estimated kinetic parameters for N_2O formation during NH_3-SCR.

Reaction	Equation/reaction rate	Pre-exponential factor[a] (kmol/(m^3 s))	Activation energy (kJ/mol)
N_2O formation (direct—high temperature)	$2NH_3\text{-}S1 + 2NO + O_2 \rightarrow N_2O + N_2 + 3H_2O + 2S1$ (r.5) $r_5 = k_5 \times \theta_{S1-NH_3} \times [NO] \times [O_2]$	1.7×10^{16}[b]	140.0 [35]
N_2O formation (indirect—low temperature)			
Surface complex formation	$NH_3\text{-}S1 + NO \rightarrow S1\text{-}NH_3\text{-}NO$ (r.6f) $r_{6f} = k_{6f} \times \theta_{S1-NH_3} \times [NO] \times \theta_v$	1×10^{4}[b]	0 [35]
Surface complex dissociation	$S1\text{-}NH_3\text{-}NO \rightarrow NH_3\text{-}S1 + NO$ (r.6b) $r_{6b} = k_{6b} \times \theta_{S1-NH_3\,NO}$	1×10^{8}[b]	34.0 [35]
Surface complex decomposition	$2S1\text{-}NH_3\text{-}NO + O_2 \rightarrow N_2O + N_2 + 3H_2O + 2S1$ (r.7) $r_7 = k_7 \times \theta_{S1-NH_3\,NO} \times [O_2] \times \theta_v$	2×10^{6}[b]	29.0 [35]

[a] The unit for the reaction rate is kmol/(m^3 s) and the gas phase concentrations are dimensionless.
[b] Fitted.

from the inlet to the outlet. The operating temperature has a major effect on the NH_3 surface coverage since desorption becomes faster at higher temperature and the equilibrium is shifted towards the gas phase. The NH_3 SCR reaction also occurs at a higher rate when the temperature rises. In addition, ammonia oxidation might occur, although the rate compared to SCR was significantly lower in the interval studied. A correlation can be established between the location where the NH_3 coverage reaches zero and the location where NH_3 is fully consumed, at all three temperatures. At 200 °C (Fig. 6), the ammonia coverage was near zero close to the outlet where the ammonia gas phase concentration was zero; note that the distributions in the rear of the catalyst are limited by the reported data density and that the actual distribution in this region is not expected to be linear. At 325 °C (Figure 6), the null ammonia coverage and ammonia concentration were observed from 3/16 of the total length. The coverage at 400 °C was very close to zero already at the inlet position (Fig. 6). At 200 °C, the NH_3 coverage was over 0.5 in the entire front half while at 325 °C, it was significant only in the front of the SCR catalyst. These coverage simulation results are consistent with our experimental measurements of distributed coverage at 200 and 325 °C in terms of both shape and spatial extent [cf. Fig. 9 and associated discussion in reference [12]].

4.6. N_2O formation

NH_3-SCR catalysts convert NO into N_2 and may produce N_2O as a side product. N_2O formation should be minimized to obtain the N_2 selectivity as close to 100% as possible. The Cu-BEA catalyst tested in the present study produced N_2O during SCR in various proportions depending on the temperature (Fig. 7). The outlet N_2O concentration was 18 ppm at 200 °C, 11 ppm at 325 °C and 15 ppm at 400 °C. The production of N_2O has therefore no linear temperature dependence and cannot be explained by only one reaction following Arrhenius' kinetic law. Instead, the N_2O concentration is higher at 200 and 400 °C than at 325 °C, describing two peaks of formation, at low and high temperature. Delahay et al. [11] correlated the presence of CuO aggregates to the low temperature N_2O formation. Centi et al. [38] suggested that N_2O formation originates from the decomposition of ammonium nitrate intermediate, at low temperature. At high temperature, Delahay et al. [11] postulated copper ions or copper dimers $[CuOCu]^{2+}$ as active species in the formation of N_2O. Thus, two paths are proposed to model N_2O formation and a mechanism developed by Supriyanto et al. [35] was used in this study. The low temperature path involves the formation of a surface NH_3-NO complex that decomposes into N_2O. This complex is, in the model, formed on the sites S1 (see Table 5, r6f). This complex formation is reversible and the backward reaction, r6b, is also shown in Table 5. The reversibility is crucial for describing the lower N_2O formation at 325 °C. The NH_3-NO complex can also decompose to form N_2O (see Table 5, r7). The lower thermal stability of the NH_3-NO complex at 325 °C vs. 200 °C is the reason for the lower N_2O at 325 °C in the model, which is in agreement with the measurements. The second N_2O formation path is active at high temperature and has therefore a high activation barrier. It consists of the reaction of NH_3 adsorbed on S1 sites with gas phase NO and O_2 to produce N_2O; this is shown in Table 5 as the 'direct—high temperature' reaction. Since this is a global reaction step, gas phase NO and O_2 were used for simplification. However, the real mechanism functions through adsorbed species. By using these two N_2O mechanisms, it was possible to account for the relatively high N_2O formation at low (200 °C) and high (400 °C) temperatures and the lower production at intermediate temperature (325 °C). The reaction equations and optimized kinetic parameters are reported in Table 5, where the activation energies were taken from Supriyanto et al. [35] (Table 6).

The results in Fig. 7 suggest that N_2O formation, like the SCR reaction, becomes faster when the temperature increases. Indeed, the slope of the N_2O profile at the catalyst inlet increases with temperature. However, the outlet N_2O concentration did not follow the temperature since the highest integral N_2O production occurred at 200 °C (Fig. 7a) and the lowest at 325 °C (Fig. 7b), as previously discussed. At 200 °C, the low temperature route mostly contributes to N_2O production whereas at 400 °C, the N_2O profile was not affected by the low temperature mechanism. The N_2O profiles, calculated by our model, well match the experimental profiles at all three temperatures.

4.7. Model validation: 4-step protocol transient behavior

The transient aspects of the 4-step protocol were used to validate the model. Each step showed transient phenomena like NH_3 storage (Steps 2 and 3), non-steady state reaction (all steps) and the reaction between gas species and stored species (Step 4). The full transient protocol was simulated using the optimized kinetic parameters fitted to the steady state intra-catalyst axial concentration profiles. The NO, NH_3, N_2 and N_2O profiles at 0.5L and 200 °C were compared to the simulation results (Fig. 8). The comparison is shown for position 0.125L and 0.25L at 325 °C (Fig. 9) and 400 °C (Fig. 10), respectively. The results shown are representative of different settings, namely temperature and axial position. In addition, these positions are all within the SCR zone of the catalyst at their respective temperature, which means that the NH_3 concentration during the SCR step was not null and can be compared. The variance was calculated over each step and reported in Table 7. In the first example, at 200 °C and 0.5L, the model yields excellent agreement with the experiments (see Fig. 8). At this position, both the steady-state spatial profiles and the transient curves of NO (a), NH_3 (b), N_2 (c) and N_2O (d) match well. In the first step, NO oxidation was not significantly occurring, which was accurately described by the model. Thereafter, ammonia was added to the feed gas mixture, resulting in the SCR reaction. Large ammonia storage is apparent. Since the ammonia coverage was increasing during Step

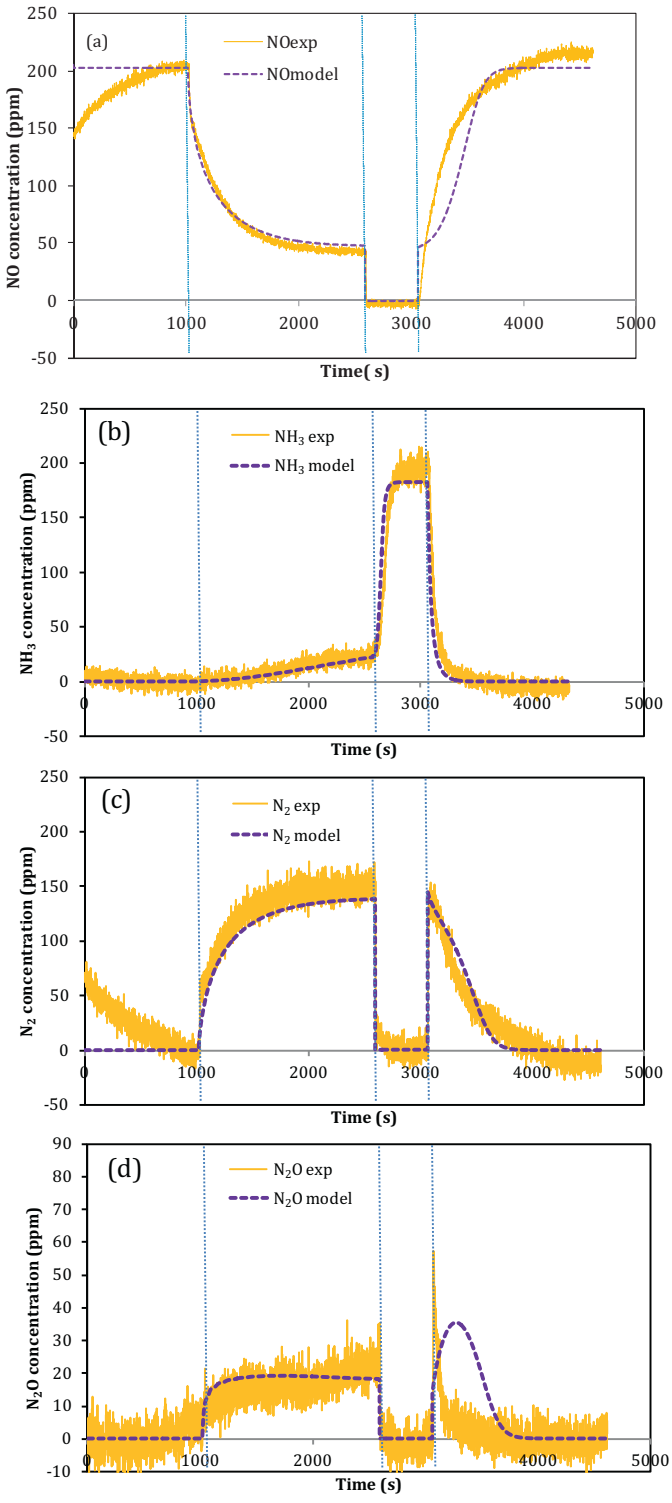

Fig. 8. Full transient 4-step protocol as model validation: experiment (solid lines) and simulation (dashed lines) intra-catalyst concentration profiles at 200 °C and 0.5L location; the three vertical dashed lines indicate the progressive transition times between protocol steps 1–4: (a) NO, (b) NH_3, (c) N_2 and (d) N_2O.

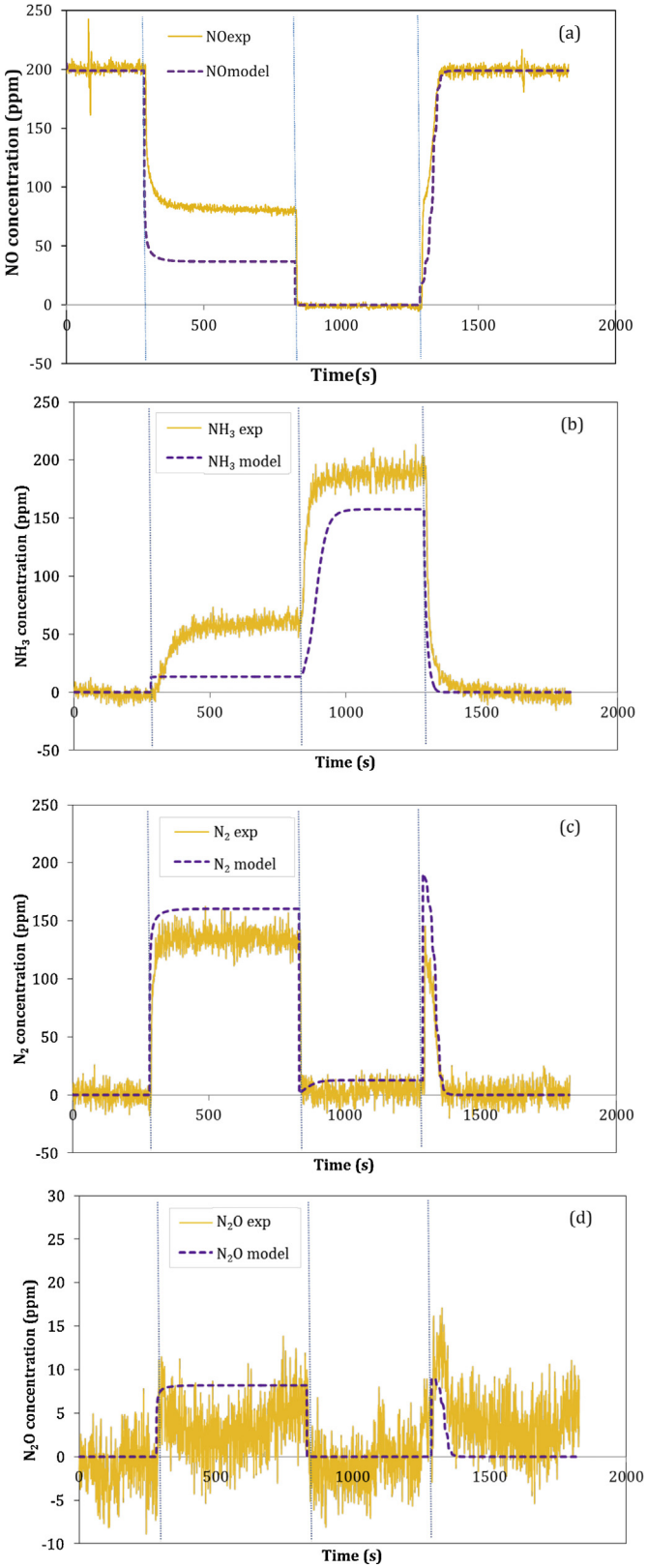

Fig. 9. Full transient 4-step protocol as model validation: experiment (solid lines) and simulation (dashed lines) intra-catalyst concentration profiles at 325 °C and 0.125L location. (a) NO, (b) NH_3, (c) N_2, (d) N_2O.

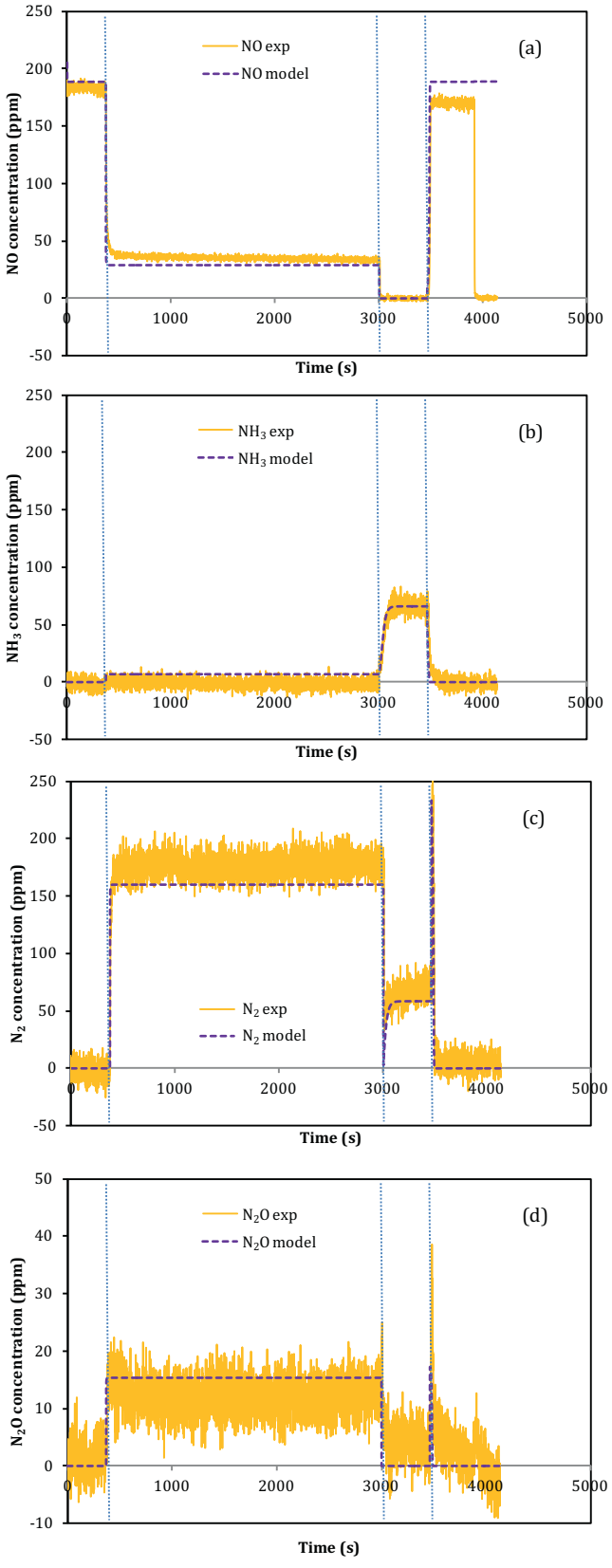

Fig. 10. Full transient 4-step protocol as model validation: experiment (solid lines) and simulation (dashed lines) intra-catalyst concentration profiles at 400 °C and 0.25L location: (a) NO, (b) NH_3, (c) N_2 and (d) N_2O.

Table 7
The variance of the transient experiment, calculated for each of the four steps.

Step	200 °C 0.5L	325 °C 0.125L	400 °C 0.25L
1-NO oxidation	4[a]	20	29
2-SCR	72	1145	111
3-NH_3 oxidation	205	1433	82
4-NO oxidation	269	261	80

[a] Variance measured over the last 5 min of the step.

2, the reaction rate for SCR was increasing. This reaction resulted in an increased NO conversion with time, which the model well predicted. In addition N_2O was observed during this step. In Step 3, NO was turned off and further ammonia storage was visible followed by a breakthrough. In Step 4, ammonia was shut off and NO started, causing the stored ammonia to react with NO to form N_2 and N_2O. The N_2O peak and the NO consumption were overestimated, which increased the variance (Table 7) but in general, the model well described the transient features of the four-step protocol, as confirmed by the low variance (Table 7).

At 325 °C and the 1/8L position (Fig. 9), the model had too high ammonia SCR rate illustrated by the lower steady-state concentrations of NO and NH_3 (Fig. 5b). The slight overproduction of N_2 in Step 2 and Step 4 is consistent with this prediction. NH_3 oxidation was also overestimated using an activation energy of 99.5 kJ/mol [34], as shown by the NH_3 level during Step 3 in Fig. 4b. These variances are consistent with the steady-state spatial results in Figure 5. With a variance greater than 1000, one can conclude that the accuracy of the model was less good for the Steps 2 and 3 at 325 °C and at the 1/8 position. Nonetheless, the transient progression of the three species to reach steady state was in good agreement with the experimental profiles during all four steps. The concentration profile features for N_2 were particularly well-captured by the model. The N_2 peak at the beginning of Step 4 well matched the experiment and the N_2 level during SCR was also close to the experimentally measured values. N_2O was well-described by the simulation in Step 4 (Fig. 9d) at 325 °C, as shown by the appearance of the characteristic peak immediately after the change of the gas composition. This peak at the beginning of Step 4 is the result of NO in Step 4 reacting with the large quantity of stored ammonia on the catalyst surface from Step 3 to form N_2 and N_2O until the surface ammonia is depleted.

Fig. 10 shows the experimental and simulated concentrations at 400 °C after the front quarter of the catalyst. The transient concentration changes were again captured well by the model. The steady state concentrations of all compounds including N_2O were in general agreement with the experiments during SCR and consistent with the steady state spatial results in Fig. 5. Note that, at this high temperature, the coverage of ammonia (Fig. 6) on the surface is low, which results in rapid outlet gas changes when changing the inlet gas composition, which was not the case at low temperature (compare to Fig. 8). The variance calculated at 400 °C was low for all four steps (Table 7).

5. Conclusions

The NH_3-SCR of NO over a honeycomb-monolith-supported Cu-BEA catalyst was modeled at three temperatures: 200, 325 and 400 °C. In this study, intra-catalyst spatially resolved gas composition data were used instead of integral effluent values to determine the kinetic parameters of various reactions. The kinetic parameters of NH_3 adsorption and desorption were determined through an ammonia TPD experiment and previous calorimetric measurement. NO oxidation was described by a global reaction depending on NO and oxygen concentration. In addition, the spatial profile of NH_3 oxidation was modeled separately. These submodels were

used together when the simulation of NH_3-SCR was performed. Reactions involving NO_2 were not considered in this model due to low NO oxidation activity and only NO in the feed was used. The steady state concentration of NH_3, NO and N_2 at different positions along the catalyst during NH_3-SCR was well predicted by the model.

Two routes were envisaged to model the N_2O formation. To predict the low temperature N_2O production, the formation of a surface complex was proposed. According to this route, N_2O production decreases with temperature due to thermal decomposition of the NH_3-NO surface complex, which agrees well with the lower N_2O concentration at 325 °C. The reaction between NO, NH_3 and O_2 yielding N_2O with the adequate stoichiometry represents the second route and is responsible for the N_2O production at high temperature.

To validate the model, the entire experiment, composed of a series of concentration steps, was simulated. The model could reproduce, with a good temporal agreement, the transition from NO oxidation (Step 1) to SCR (Step 2), the NH_3 storage in the NH_3 oxidation step (Step 3) following the SCR step and the reduction of NO by the stored ammonia in Step 4 ($NO + O_2 + H_2O$), yielding a characteristic N_2 and N_2O puff.

Acknowledgements

This work is a collaboration between Oak Ridge National Laboratory, Competence Centre for Catalysis at Chalmers University and Cummins Inc. This research was sponsored by the U.S. Department of Energy, Office of Energy Efficiency and Renewable Energy, Vehicle Technologies Office, with Ken Howden and Gurpreet Singh as the Program Managers and the Swedish Foundation for Strategic Research (F06-0006).

Notice: This manuscript has been authored by UT-Battelle, LLC, under Contract No. DE-AC05-00OR22725 with the U.S. Department of Energy. The United States Government retains and the publisher, by accepting the article for publication, acknowledges that the United States Government retains a non-exclusive, paid-up, irrevocable, world-wide license to publish or reproduce the published form of this manuscript, or allow others to do so, for United States Government purposes.

References

[1] T. Komatsu, M. Nunokawa, I.S. Moon, T. Takahara, S. Namba, T. Yashima, J. Catal. 148 (1994) 427–437.
[2] B. Coq, S. Kieger, G. Delahay, D. Berthomieu, A. Goursot, A new mechanism for the selective catalytic reduction of NO_x by NH_3 on Cu-zeolite catalysts (2000) 1481–1486.
[3] M. Devadas, O. Kröcher, M. Elsener, A. Wokaun, N. Söger, M. Pfeifer, Y. Demel, L. Mussmann, Appl. Catal. B: Environ. 67 (2006) 187–196.
[4] O. Kröcher, M. Devadas, M. Elsener, A. Wokaun, N. Söger, M. Pfeifer, Y. Demel, L. Mussmann, Appl. Catal. B: Environ. 66 (2006) 208–216.
[5] H. Sjövall, L. Olsson, E. Fridell, R.J. Blint, Appl. Catal. B: Environ. 64 (2006) 180–188.
[6] A. Grossale, I. Nova, E. Tronconi, Catal. Today 136 (2008) 18–27.
[7] K. Rahkamaa-Tolonen, T. Maunula, M. Lomma, M. Huuhtanen, R.L. Keiski, Catal. Today 100 (2005) 217–222.
[8] M. Koebel, G. Madia, M. Elsener, Catal. Today 73 (2002) 239–247.
[9] A. Grossale, I. Nova, E. Tronconi, D. Chatterjee, M. Weibel, J. Catal. 256 (2008) 312–322.
[10] C. Ciardelli, I. Nova, E. Tronconi, D. Chatterjee, T. Burkhardt, M. Weibel, Chem. Eng. Sci. 62 (2007) 5001–5006.
[11] G. Delahay, B. Coq, S. Kieger, B. Neveu, Catal. Today 54 (1999) 431–438.
[12] X. Auvray, W.P. Partridge, J.-S. Choi, J.A. Pihl, A. Yezerets, K. Kamasamudram, N.W. Currier, L. Olsson, Appl. Catal. B: Environ. 126 (2012) 144–152.
[13] J.-Y. Luo, H. Oh, C. Henry, W. Epling, Appl. Catal. B: Environ. 123–124 (2012) 296–305.
[14] J.-Y. Luo, X. Hou, P. Wijayakoon, S.J. Schmieg, W. Li, W.S. Epling, Appl. Catal. B: Environ. 102 (2011) 110–119.
[15] B. Roduit, A. Wokaun, A. Baiker, Ind. Eng. Chem. Res. 37 (1998) 4577–4590.
[16] H. Sjövall, R.J. Blint, A. Gopinath, L. Olsson, Ind. Eng. Chem. Res. 49 (2010) 39–52.
[17] L. Olsson, H. Sjövall, R.J. Blint, Appl. Catal. B: Environ. 81 (2008) 203–217.
[18] S. Shwan, J. Jansson, J. Korsgren, L. Olsson, M. Skoglundh, Catal. Today 197 (2012) 24–37.
[19] H. Sjovall, R.J. Blint, L. Olsson, J. Phys. Chem. C 113 (2009) 1393–1405.
[20] H. Sjövall, R.J. Blint, L. Olsson, Appl. Catal. B: Environ. 92 (2009) 138–153.
[21] L. Olsson, H. Sjövall, R.J. Blint, Appl. Catal. B: Environ. 87 (2009) 200–210.
[22] S. Shwan, W. Partridge, J.-S. Choi, L. Olsson, Appl. Catal. B: Environ. (2014).
[23] N. Wilken, K. Kamasamudram, N.W. Currier, J. Li, A. Yezerets, L. Olsson, Catal. Today 151 (2010) 237–243.
[24] K.W.N. Wilken, K. Kamasamudram, N.W. Currier, R. Vedaiyan, A. Yezerets, L. Olsson, Appl. Catal. B: Environ. (2011).
[25] J.-S. Choi, W.P. Partridge, C.S. Daw, Appl. Catal. A: Gen. 293 (2005) 24–40.
[26] J.-S. Choi, W.P. Partridge, C.S. Daw, Appl. Catal. B: Environ. 77 (2007) 145–156.
[27] J.-S. Choi, W.P. Partridge, W.S. Epling, N.W. Currier, T.M. Yonushonis, Catal. Today 114 (2006) 102–111.
[28] W.P. Partridge, J.-S. Choi, Appl. Catal. B: Environ. 91 (2009) 144–151.
[29] W.P. Partridge, T.J. Toops, J.B. Green, T.R. Armstrong, J. Power Sources 160 (2006) 454–461.
[30] K. Kamasamudram, N.W. Currier, X. Chen, A. Yezerets, Catal. Today 151 (2010) 212–222.
[31] AVL, BOOST aftertreatment BOOST manual, 2011.
[32] P.S. Metkar, M.P. Harold, V. Balakotaiah, Chem. Eng. Sci. 87 (2013) 51–66.
[33] S.A. Stevenson, J.C. Vartuli, C.F. Brooks, J. Catal. 190 (2000) 228–239.
[34] O. Mihai, C.R. Widyastuti, S. Andonova, K. Kamasamudram, J. Li, S.Y. Joshi, N.W. Currier, A. Yezerets, L. Olsson, J. Catal. 311 (2014) 170–181.
[35] Supriyanto, A. Kumar, S. Joshi, K. Kamasamudram, N.W. Currier, A. Yezerets, L. Olsson, Appl. Catal. B (2014), http://dx.doi.org/10.1016/j.apcatb.2014.07.059.
[36] N. Wilken, K. Wijayanti, K. Kamasamudram, N.W. Currier, R. Vedaiyan, A. Yezerets, L. Olsson, Appl. Catal. B: Environ. 111–112 (2012) 58–66.
[37] P.S. Metkar, V. Balakotaiah, M.P. Harold, Catal. Today 184 (2012) 115–128.
[38] G. Centi, S. Perathoner, D. Biglino, E. Giamello, J. Catal. 152 (1995) 75–92.